Accepted Manuscript

Title: Selective contrast agents with potential to the earlier detection of tumors: Insights on synthetic pathways, physicochemical properties and performance in MRI assays

Authors: María Gabriela Montiel Schneider, María Julia Martin, Diego Coral, Diego Muraca, Claudia Gentili, Marcela Fernández van Raap, Verónica Leticia Lassalle

Please cite this article as: Schneider MGM, Martin MJ, Coral D, Muraca D, Gentili C, van Raap MF, Lassalle VL, Selective contrast agents with potential to the earlier detection of tumors: Insights on synthetic pathways, physicochemical properties and performance in MRI assays, *Colloids and Surfaces B: Biointerfaces* (2018), https://doi.org/10.1016/j.colsurfb.2018.06.044

Selective contrast agents with potential to the earlier detection of tumors: Insights on synthetic pathways, physicochemical properties and performance in MRI assays

María Gabriela Montiel Schneider[1]; María Julia Martin[2]; Diego Coral[3,4], Diego Muraca[5], Claudia Gentili[2], Marcela Fernández van Raap[3], Verónica Leticia Lassalle[1,*]

[1]INQUISUR, Departamento de Química, Universidad Nacional del Sur (UNS)-CONICET, Av. Alem 1253, 8000 Bahía Blanca, Argentina
[2]INBIOSUR, Departamento de Biología, Bioquímica y Farmacia, Universidad Nacional del Sur (UNS)-CONICET, San Juan 671, 8000, Bahía Blanca, Argentina.
[3]Instituto de Física La Plata IFLP-CONICET, Departamento de Física, Universidad Nacional de La Plata, La Plata, Buenos Aires, Argentina
[4]Institución Universitaria CESMAG, Pasto-Colombia
[5]Laboratório de Materiais e Dispositivos, Instituto de Fïsica 'Gleb Wataghin', Universidade Estadual de Campinas, Campinas, Brazil

*Address for Correspondence:
Dra. Verónica Lassalle, Dpto. de Química, INQUISUR
Universidad Nacional del Sur-CONICET
Avda. Alem 1235, (B8000CPB) Bahía Blanca, Bs. As., Argentina
+54 291 4595101 int. 3534.
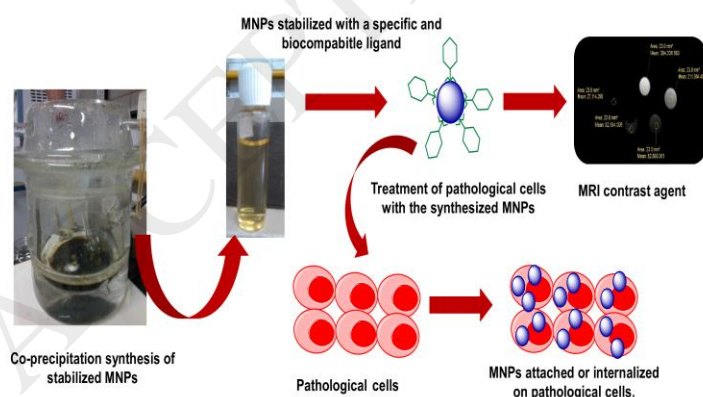veronica.lassalle@uns.edu.ar

Statistical summary:
 Words 5021
 Tables: 2; Fig.1(a+b); Fig. 2; Fig. 3 (a+b); Fig. 4(a+b) Fig. 5(a+b); Fig. 6(a+b)
Total:8

Graphical abstract

Highlights

- Screening synthesis conditions to attain MRI contrast agents for tumors detection.
- Ascorbic acid coated magnetite (Mag-AA) was the most stable formulation.
- MRI using clinical equipment suggests Mag-AA is efficient as T2 contrast agent.
- Cell viability and up take on human colon cancer cells shows satisfactory results.

Abstract

Magnetic iron oxide nanoparticles (MNPs) have been prepared and stabilized with three organic acids (tartaric, malic and ascorbic) in order to obtain biocompatible and water dispersible MNPs with potential to bind specifically to tumoral cancer cells. An in deep characterization was performed aiming to verify the presence and effect of the coating and stabilizer on MNPs surface. Besides the mechanisms followed by the different acids to bind MNPs were elucidated and used to justify the differences in the physicochemical properties of each formulation. Data related to characterization revealed that MNPs coated ascorbic acid (MNPs-AA) resulted the most suitable in terms of their size, surface charge and stability along the time. Besides, ascorbic acid may be recognized by GLUTs receptors that are overexpressed in several kinds of tumoral cells. Therefore, MNPs-AA was selected to explore its performance in both MRI and in vitro assays using human colon cancer cells HCT 116. MRI experiments were performed in clinical equipment using a series of aqueous dispersions of MNPs-AA that were evaluated as T_2 contrast agent. The T_2- weighted images obtained as well as the calculated r2, indicated that MNPs-AA could act as efficient T_2 contrast agent for MRI.

Regarding in vitro assays, MNPs-AA did not alter the cellular function neither exert cytotoxicity using the three explored doses. The internalization of the nanoparticles on the cellular structure was confirmed quanti and qualitatively using atomic absorption spectroscopy and Prussian blue techniques respectively.

From these results, it emerges that ascorbic acid coated-magnetite nanoparticles may be used as alternative contrast agent to avoid or minimize some toxicological issues related to the widely used gadolinium.

1. Introduction

An urgent need for achieving early and selective diagnosis is actually recognized due to the severity of many pathologies such as cancer and cardiovascular diseases [1,2] .

At present, gadolinium derivatives are almost exclusively employed as contrast agent (CA) for MRI and have generally been considered safe when administrated in chelate forms. However, the use of gadolinium has been restricted in patients with acute renal dysfunction because of the risk of develop nephrogenic systematic fibrosis, in child and in other groups of health vulnerable patients [3,4]. In this view, MNPs with optimal characteristics, in terms of the contrast capability, size and size distribution, may be taken as a valid and safe alternative with these groups of patients [5,6].

In fact, the application of iron oxide magnetic nanoparticles as CA have been widely reported, in particular as T_2 CA [7]. In this concern, several CA based on iron oxides have been available in the market since the earlier 90´. Although most of them have been actually discontinued or withdrawn from the market for multiple reasons [8]. The possibility to coat the MNPs providing selectivity for a specific target, represents a great advantage regarding to the efficiency of these nanosystems to the early detection of diverse pathologies. Besides, recent literature is focusing on the dual capability of MNPs in the therapy and diagnostic of oncological diseases [9].

It has been proposed that nanoparticles intended for the recognition of cell surface receptors may represent an attractive way to the identification of tumor cells using MRI techniques[10].

For example, magnetic nanoparticles were modified with hyaluronic acid as a selective ligand to CD44 receptors, which are overexpressed in different kind of cancer cells. In this way it would be possible the sensitive detection of such tumor cells [11,12]. Hyaluronic acid coated magnetic nanoparticles have also been studied for imaging atherosclerosis [13]. The folate receptor is another interesting target because is overexpressed in cancer cells and activated macrophages. Liu et al conjugated folic acid to magnetic nanoparticles and succeeded in the separation of metastatic ovarian cancer cell from the bloodstream, despite the low concentration of them in blood [14]. Other recent studies involve the use of different compounds promoting specific interactions with receptors overexpressed in several pathologies aiming to assess an early detection by MRI [15,16].

The aim of this work is to design MNPs with suitable properties able to be employed as contrast agents to assess the earlier diagnostic of high impact diseases, such as cancer, by MRI. To do this, magnetite nanoparticles were coated with: ascorbic, tartaric and malic acids. Since they are non-toxic compounds [17–19], biocompatible and hydrophilic nanoparticles could be obtained. In particular ascorbic acid deserves special

interest as a water-soluble vitamin with several implications in human health [19]. According to reported literature, numerous tumor cells overexpress the glucose transporters (GLUTs) which are implicated in the accumulation of ascorbic acid in tumors [20]. The mechanisms proposed for this accumulation include the extracellular oxidation of ascorbic to dehydroascorbic acid and the transportation of this form inside the tumor cell by the GLUTs transports. Once into the cell, dehydroascorbic acid is reduced and remains in its interior [21].

In this context, this contribution proposes a rigorous study of the synthetic pathways to achieve coated MNPs potentially useful as CA with suitable properties to be selectively employed in tumor detection by MRI. The performance of MNPs as contrast agents for MRI was studied using clinical equipment; whereas their cytotoxicity and internalization capability were assessed on HCT116 cells derived from human colon carcinoma.

2. EXPERIMENTAL

2.1. Materials

All reagents were of analytical grade and used without further purification. Ferric chloride hexahydrate was provided by Biopack (Argentina), ferrous sulphate heptahydrate was provided by Mallinckradt Chemical Works (USA). Sodium hydroxide was purchased from Cicarelli (Argentina).

2.2. Methods

2.2.1-Synthesis of Magnetic Nanoparticles

The magnetite nanoparticles were synthesized by co-precipitation with some modifications regarding to the traditional methodology based on previous own works [22,23]. Briefly, 0.358 g of $FeSO_4$ and 0.651 g of $FeCl_3$ were dissolved in 20 ml of distilled water in a thermostatized reactor at 60ºC under nitrogen atmosphere. A stabilizer was added to the Fe^{2+}/Fe^{3+} aqueous solution (an organic acid or PEG, see Table S1). Then, an alkali solution was employed to precipitate magnetite. The resulting suspension was stirred during 45 minutes. The purification was assessed by cycles of washing with distilled water and magnetic decantation until pH and conductivity reached

the levels roughly comparable with the one corresponding to distilled water. This allows inferring that not free acids or alkali ions were present in the supernatant, so that the obtained coated-magnetic nanoparticles were purified.

The particular experimental conditions applied to prepare tartaric (Mag-TA); malic (Mag-MA) and ascorbic acid (Mag-AA1) coated-magnetite are depicted in supplementary material.

2.3.   Characterization

Fourier Transform Spectroscopy (FTIR) spectra were recorded in a Thermos Scientific Nicolet iS50 in the frequency range of 400-4000 cm^{-1}, using the KBr pellet method. Transmission Electron Microscopy (TEM, JEOL 100 CX II, Tokyo, Japan) was used to determine particle size and morphology of the nanoparticles. HRTEM images were achieved on a TEM-FEG (JEM 2100F) field-emission gun transmission electron microscope (voltage: 200 V, spot size 3). The images where acquired using a Gatan 831.J45M0 camera at different resolution. The images where analyzed using ImageJ free software.

X-ray diffraction (XRD) pattern of the nanoparticles were recorded using Cu-K$_\alpha$ radiation on Rigaku D-Max III-C diffraction spectrometer with a graphite monochromator.

Thermogravimetric analysis (TG) was performed in a TA Q600 equipment. Samples were weighted (30 mg) and heated at room temperature up to 650ºC at a rate about 10ºC/min under air atmosphere.

Data on hydrodynamic diameter and Z potential (ζ) were acquired in a Malvern Zetasizer (Nano-Zs90). Samples were dispersed in distilled water and sonicated for one hour before performing the acquisition.

Magnetic measurements were performed using vibrating sample magnetometer (VSM) LakeShore 7404 operated with maximum applied fields $\square$ 0Hmax= 1.8 T.

2.4.   Magnetic Resonance Imaging (MRI)

Contrast studies were performed in a clinical whole-body MRI scanner (Philips Achieva 1,5T). The MNPs sample was diluted in bidistilled water to obtain suspensions in the range from 0.5 to 0.6 mmol of Fe/ml. T_2 weighted images was acquired using spin

echo (SE) pulse sequence. The time echo (TE) was ranged between 80 and 350 ms and the TR was maintained constant at 4000 ms.

2.5. In vitro assays

2.5.1. Cell culture

The human colorectal cell line HCT116 (from the American Type Culture Collection, Manassas, Virginia) was cultured at 37 °C in DMEM (Sigma-Aldrich Chemical Co., St. Louis, Missouri, USA) containing 10% FBS (Natocor, Córdoba, Argentina), 1% non-essential acids, 100 UI/mL penicillin, 100 mg/mL streptomycin and 50 mg/mL gentamycin in a humid atmosphere of 5% CO_2 in air. Cultures were treated every 2 days with fresh medium. All experiments were performed using passages less than 15. Cells were incubated in presence/absence of MNPs (which were previously sterilized by UV irradiation) at different concentrations.

2.5.2. Cytotoxicity evaluation

The impact of MNPs on the viability of HCT116 cells culture was evaluated using a standard MTS cell viability assay (Promega, Madison, WI). Briefly, cells were seeded for quadruplicate in 96 well plates at 2 ×10^3 cells/well. Culture medium was removed and replaced by a suspension of MNPs (1, 10 or 100 µg Fe/ml) in DMEM 10% SFB. After incubation, the culture medium was removed, replaced by fresh–DMEM without phenol red (Sigma-Aldrich Chemical Co., St. Louis, Missouri, USA) containing 10 µl of MTS reagent and after 10 minutes, the absorbance at 490 nm was recorded using a Biotek Synergy HT MicroplateReader.

2.5.3. Internalization measurements

a- Qualitative internalization assays by Prussian blue staining

2 x 10^4 HCT116 cells were grown in coverslips, for 24 hours, and incubated with a suspension of MNPs (10 or 100 µg Fe/ml) carried in fresh culture medium, during 24hs. Cells were washed and fixed with 4% paraformaldehyde and exposed to 5%

$K_4Fe(CN)_6$/1% HCl and counterstained with Giemsa. Slides were observed using an optic microscope equipped with an Olympus camera.

b-Quantitative internalization by Atomic absorption measurements

The presence of MNPs on the cells was determined by measuring the Fe content.7 x 10^4 HCT116 cells/well were grown in 6-well plates, and incubated with a suspension of MNPs (1, 10 or 100 µg Fe/ml). After 24 hours, the supernatant of each well was collected and treated with HCl 10%. Cells were detached from the wells with trypsin, resuspended and centrifuged. Cells supernatant and cell pellets were treated with HCl 10%. The solutions were sonicated to ensure that all iron was released from magnetite. Afterwards, iron concentration was measured for each fraction by atomic absorption spectroscopy. Finally, cellular uptake of MNPs was calculated from the internalized amount of MNPs normalized to the total incubated amount of MNPs, both expressed as µg of MNPs, according the following formula:

%Cellular uptake = Internalized amount of MNPs x100/ Total incubated amount of MNPs

3. Results and discussion

3.1. Synthesis and characterization of magnetic nanoparticles

3.1.1. FTIR analysis

Figure 1a shows IR spectra of three raw acids and **Figure 1b** those corresponding to MAG coated with TA, MA and AA respectively. The spectrum of Mag-TA confirming the incorporation of the organic acid on the iron surface by the presence of carbonyl band assigned to the acid. The stretching signal of C=O shifted from 1734 cm^{-1} in pure tartaric acid to 1648 cm^{-1} in Mag-TA, revealing that the interaction is given by C=O acidic group and Fe atoms in the particles surface [24].

The stretching band of C-O corresponding to the alcohol functional group at 1060 cm^{-1} is also observable in Mag-TA spectrum. Whereas the stretching band of Fe-O from iron oxide appears at 592 cm^{-1}.

Comparing the spectra of Mag-MA with the corresponding to raw MA, it may infer that the MA was linked to the magnetite surface. The signal of C=O assigned to MA is observed in Mag-MA spectrum although shifted to lower wavenumber (1625 cm^{-1}) with respect to MA spectrum (1740 cm^{-1}). This may be due to MAG interactions. Two bands at 1384 and 1054 cm^{-1} are also distinguished and may be ascribed to the stretching vibrations of C-H and C-O respectively.

From IR spectra of pure ascorbic acid and Mag-AA1, it is possible observe that the stretching vibration of C=O group of ascorbic acid observed at 1756 cm^{-1} in raw AA, is also shifted to 1631 cm^{-1} in Mag-AA1, indicating the surface MAG modification. It is worth noting that C=C signal appears at 1675 cm^{-1} in AA spectrum, but it is not clearly distinguished in Mag-AA1 spectrum. This could be due to the reduction of the C=C to form the dehydroascorbic acid [25]. It is also feasible that C=C band overlaps with the corresponding to C=O, limiting its detection.

Besides, other bands corresponding to the stretching vibration of O-H at 3409 cm^{-1}, stretching of C-H at 2930 cm^{-1} and those associated to the deformation vibration of C-H at 1389-1324 cm^{-1} may be distinguished in the spectrum of Mag-AA1. The signals observed at 1120 and 1014 cm^{-1} ascribed to alcoholic C-O, in combination with those earlier described, reveal the effective incorporation of AA on the MAG surface[25]. The typical Fe-O band from magnetite is also observed around 583cm^{-1}.

3.1.2. *Measurements of Z potential, hydrodynamic diameters and morphology by TEM*

The hydrodynamic diameter and z potential data of the coated-MNPs as well as naked magnetite are listed in **Table 1**. Data on the Table indicate a high reduction of the hydrodynamic diameter because of the organic acids coating on MAG surface. These findings highlight the stabilizing effect of the selected acids on the MAG in aqueous dispersion.

The zeta potential of the samples was measured at pH 6.1-6.8 and provides information about the surface charge of MNPs. Hence, it may be taken as a measurement of the stability of colloidal dispersion, since it is responsible for the degree of electrostatic repulsive forces between particles. Therefore, the increment in magnitude observed in coated MNPs in relation to naked magnetite, suggests that an effective electrostatic

stabilization was achieved. The enhanced in the negative ζ value is in agreement with the presence of carboxylate groups in MNP surface.

It is worth mention that both, TA and MA, have two carboxylic acids groups with pKas around 3.04 and 4.37; and 3.4 and 5.11, respectively [26,27].
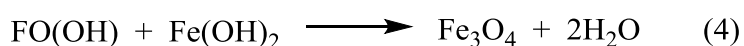
The ζ value of Mag-AA is related to the presence of two ionizable hydroxyl groups, one of them with a pKa 4.2 [28]. These results confirm the presence of the acid in the magnetic iron oxide surface, supporting the FTIR data.

Regarding to the morphology, all prepared MAG formulations resulted almost spherical and uniform in shape, as it is observed in **Figure 2**. Noticeable differences are appreciated by comparing the sizes estimated by dynamic light scattering and TEM, respectively. This is consistent with the principle of each method, considering that the hydrodynamic sizes are recorded by DLS and include the measure of aggregates of nanoparticles in dispersion [22].

Table 1. Data on hydrodynamic size, TEM estimated size and ζ, as a function of the coating.

3.1.3. Thermal analysis and XRD data

The magnetite crystalline pattern is clearly distinguished in Mag-MA and Mag-AA1 diffractograms, as it is shown in **Figure 3a**. On the other hand, the characteristic's MAG peaks are barely distinguished in Mag-TA diffractogram (see **Figure 3a**). Broad signal was obtained, probably due to the formation of a tartrate-Fe complex, interfering in magnetite's precipitation and crystallization. Tartaric acid is recognized as iron chelating agent, favoring the occurrence of tartrate-Fe coordination bonds. The mechanism generally accepted for the formation of magnetite through the co-precipitation method is well known and described by the following equations [23]:

$$Fe^{3+} + 3OH^- \longrightarrow Fe(OH)_3 \qquad (1)$$

$$Fe(OH)_3 \longrightarrow FeO(OH) + H_2O \quad (2)$$

$$Fe^{2+} + 2OH^- \longrightarrow Fe(OH)_2 \qquad (3)$$

$$FO(OH) + Fe(OH)_2 \longrightarrow Fe_3O_4 + 2H_2O \qquad (4)$$

Tartrate ion would participate in the earlier steps, by restricting the $Fe(OH)_3$ precipitation (**Equation 1**). Hence it is possible that the formation of a mixture of Fe-tartrate species and other iron oxides occur in the alkaline reaction media [29]. In fact, the first synthesis conducted using 600 mg of tartaric acid (the same amount used for Mag-MA and Mag-AA1 synthesis) yielded a non-magnetic product. Increasing the amount of tartaric acid could favor the predominant formation of iron-complex instead of the stabilized magnetic iron oxide [30]. Other authors have reported similar observations, where the presence of analogous acids, such as oxalic in almost similar experimental conditions, rendered lepidocrosite or akageneite instead of magnetite. [31].

Thermogravimetric curves of Mag-MA (data not show included in Supplementary Material, S1) shows three steps-loss: one associated to loss of water at 100ºC; and two steps related to the decomposition of malic acid. It has been reported that MA has a wide decomposition range, ending at 275ºC [32]. In the case of Mag-MA this ending is found at 340ºC, and may be ascribed to the MA linkage on the magnetic core. Other authors have found similar trends. Prakash *et al* reported that the weight loss of MA bonded on nanocrystalline hydroxyapatite occurs between 200 and 600º [33].

From this analysis, it may infer that the mass loss associated to the organic fraction reached around 4%. This result corresponds with the one recorded by atomic absorption, that was roughly about 6%.

Thermogravimetric curves of Mag-AA1 (Figure S1b) shows the step-loss of water at 100ºC and a step-loss starting at 180ºC (the initial temperature decomposition of AA under air) [34]. The total weight loss due to the organic fraction was about 6%. From the atomic absorption measurement, it was determined that the amount of magnetite in the sample was 90%. Hence, already a 10% may be assumed that corresponds to the organic fraction, in agreement with the TG data.

3.1.4.   Magnetic measurements

The **Figure 3b** includes the data registered from VSM measurements of all the prepared MNPs. Mag-TA exhibits a very low magnetization to saturation value when compared with Mag-MA and Mag-AA whose value is almost in the range of other Mag coated nanoparticles [35–37]. This finding may be justified in terms of the formation of

other non-magnetic iron oxide such as lepidocrosite or akageneite supporting the XRD data.

Mag-MA and Mag-AA1 magnetization curves reveal a superparamagnetic behavior (**Figure 3b**). Curves were fitted with a Langevin function (red line) and negligible coercitivity is observed. This behavior is possible in nanoparticles whose size is smaller than 25 nm [38]. Superparamagnetism is an important property for MNPs intended for biological applications [39]. The magnetization to saturation values are lower than the corresponding to bare magnetite [40] due to surface coated with the organic material [40,41].

Sizes of magnetic core were estimated from VSM data following the procedure described in reference [42]. These values of about 3.7 and 3.8 nm for Mag-MA and Mag-AA1 respectively, roughly coincide with the sizes estimated by TEM as an approximation.

3.1.5. Selection of the most suitable coated MAG formulation

In view of the data arising from the characterization, it is clear that either Mag-MA or Mag-AA1 would result in efficient nanocarriers to assess both the diagnostic and subsequent target to the interest biomarkers. In spite of having similar characteristics in terms of size and zeta potential, Mag-AA1 demonstrated to be more stable in suspension than Mag-MA, over time. This last one, precipitated after 12 hours in aqueous dispersion, while Mag-AA1 kept in suspension for weeks without suffering great deviations from their original hydrodynamic size. Besides, the mechanism for AA to act as selective ligand in tumoral environment is well identified involving the interaction with GLUTs receptors overexpressed in several kinds of tumoral cells.

In this regards, a deeper study was developed aiming to ensure a suitable AA coating to the desired applications.

3.1.5.1-Influence of the initial AA concentration

The effect of different initial amounts of AA was explored aiming to: i-Ensure an enough concentration of the acid on MAG surface to accomplish the target function; ii-to improve physicochemical properties such as size, size distribution and fundamentally their stability in media simulating the physiological environment.

The **Figure 4a** depicts the evolution of Hydrodynamic diameter and Z potential as a function of the AA concentration initially added to the MAG nanoparticles. An almost linear trend between negative surface charge and AA concentration is almost observed. The negative surface charge increases with higher AA nominal concentrations. This is consistent with published works, that demonstrate that higher colloidal stabilization was achieved in aqueous media by increasing the amount of stabilizers [43,44].

On the other hand, the hydrodynamic diameter seems not to be sensitive to the variation of AA amount. The HD reaches almost a constant value by using different AA concentrations. The same is observed by examining the morphology of nanoparticles. Increasing AA nominal concentration seems not to affect the size and shape of MNPs. **Figure 4b** shows HR TEM images of MAG-AA3 to illustrate. From those images is easy to see a well spherical shape of the nanoparticles and the corresponding AA coating. In addition, no agglomerations are detected and a few nanometers distance between nanoparticles is evidenced. The high resolution microscopy also confirms the crystallinity of the particles (see **Figure 4b**). From fast Fourier transform (FFT) was possible to estimate the distance between the Bragg planes consistent with the expected for the (0,2,4) interplanar distance of Fe_3O_4.

The use of higher AA amounts did not alter the magnetic properties of nanoparticles as reveal the saturation magnetization values (Supplementary Material, S4). In fact, almost similar values were recorded in the three formulations. The magnetic core sizes determined by VSM data also resulted already constant for all AA formulations (around 4-5 nm).

The incorporation of PEG on the co-precipitation media resulted crucial to attain MAG-AA with suitable properties for biomedical intends. The addition of PEG instead of ascorbic acid to the co-precipitation media was implemented exclusively for stabilization ends. It is well known that the vitamin may reduce Fe^{3+} leading to an alteration in the Fe^{3+}/Fe^{2+} ratio required to achieve magnetite [45,46].Therefore, the coating with ascorbic acid was performed in a posterior step after the precipitation of iron oxide nanoparticles.

Findings related to FTIR reveal that PEG is not binding to the particles surface, because its stabilization mechanism is by steric hindrance in the dispersion media [43].

3.2. Magnetic Resonance Imaging (MRI)

In order to evaluate the performance of Mag-AA3 as contrast agent, T_2-weighted MRI images were explored using a series of MNPs dispersions with concentrations ranging between 0.05 to 0.6 mM Fe. These doses were selected based on published articles in open literature studying analogous nanosystems [25]. The **Figure 5a** shows the data acquired from different Mag-AA3 aqueous dispersions in T_2-weighted images. From this, it is evident that the intensity falls in T_2-weighted images as the concentration of Mag-AA3 in the dispersions increases. Darker images were obtained as the concentration of the nanoparticles increased. Signal intensity for each concentration was determined by manually drawn a region of interest (ROI). By plotting the ROI vs the TE, T_2 relaxation curves were obtained (data included in supplementary material, S6). The curve shows that as the concentration of the nanoparticles increase from 0.05 to 0.4 Mm Fe, the curve become steeper showing that Mag-AA3 is shortening the T_2 relaxation time [47,48]. Apparently, when the dose increase to 0.6 mM Fe the effect on signal intensity is lower than with the dose of 0.4 mM. To justify this behavior, the relation between signal intensity and the concentration of Mag-AA3 has to be considered (data included in supplementary material, S7). The data on the figure suggest that a reduction of 41% in signal intensity is reached by using a dispersion containing 0.05 mM Fe from Mag-AA3. The signal intensity exhibits an intense fall of about 99.25% when a dispersion of 0.2 mM of Fe is employed. In all measurements the evolution of the signal intensity was monitored using distilled water as reference. From this analysis, it may infer that using a limit concentration of 0.2 mM Fe, the system reaches an almost steady state though that signal intensity exhibits an almost constant value, independently on the dispersion concentration (see Table S3 supplementary material). In fact, the assays performed using higher concentration of dispersion (i.e 0.6Mm) leaded to inconsistent signal intensity data.

To evaluate the efficiency of MAG-AA3 to act as T_2 contrast agent, the relaxivity r2 was determined by plotting the transverse relaxation rate (1/T2) vs iron concentration. **Figure 5b** depict that the data follows a linear tendency. From this plot, the r2 value was obtained as the slope of the curve. The found relaxivity value was 198 mM^{-1}.s^{-1}, which is significantly higher than the one reported for the FDA-approved Ferumoxtran-10, whose measured relaxivity value at 1.5 T was 60 mM^{-1}s^{-1}[28,49]. The improved constrast properties, given by the high r2 value measured, may be ascribed to the physical and morphological characteristics of the MNPs. The size of MAG-AA3 is suitable to contrast in T2-weighted images [50]. Besides, as it was determined by TGA

and atomic absorption spectroscopy, the coating surrounding the magnetic core is not thicker enough. This property improved the interactions between water protons and the magnetic surface [51]. Based on the obtained data, MAG-AA3 could be considered as an efficient T2 contrast agent. These assays constitute the needed in vitro preliminary step, since were measured in simulated physiological environment.

It is worth noting that properties of these nanoparticles, such as size, are satisfactory to ensure their performance as T2 contrast agent. Examples found in open literature deal with larger nanoparticles tested as negative contrast agents. For example, Taboada et al observed that silica coated-magnetic nanoparticles with a hydrodynamic diameter of 300 nm and r2 value of 326 mM^{-1}s^{-1}exhibit a great performance as T2 contrast agent [52]. In fact, the informed r2 value corresponds to twice the value of Endorem®. The authors proposed that the largest magnetic nucleus induce larger magnetic inhomogeneities, reducing the T2 time, which may lead to a higher efficiency.

The following instance will be the *in vivo* MRI studies to corroborate their efficiency and biosafety.

In vitro assays

3.2.1.   *Biocompatibility of MNPs*

MTS was employed to evaluate cell viability after exposure to Mag-AA3. Only living cells are able to reduce the MTS. The product of such reduction may be quantified spectrophotometrically after dissolution in DMSO at 490 nm. The data obtained from this assay are considered indicators of cell survival [53].

Figure 6a shows the absorbance recorded at 490 nm using the three explored doses during two fixed times (i.e. 24 and 48hs). From the Figure appears that the cell viability was not affected by the presence of the particles after 24 and 48 hours, using any of the three assayed doses (1, 10 and 100 µg MNPs/ml).

When MNPs interact with the cell, they can influence the cellular processes, causing cell stress, by changing the metabolic activity, inducing oxidative stress and cytoskeleton disruption, or through DNA damage [54]. The toxicity of iron oxide particles varies between particle and cell type and depends on many factors, being the physicochemical properties of MNPs the key one [55]. Some discrepancies are found in open literature regarding the source of toxicity exerted by MNPs. Numerous studies

examining the impact iron oxide nanoparticles *in vitro* suggest that the toxicity is related to the nature of the coating and experimental conditions; without evidences to toxic effects induced by the magnetic core (maghemite or magnetite) [56]. On the other hand, other researchers report that the magnetic component may induce oxidative stress associated to high Fe concentrations. In general, the cytotoxicity attributed to MNPs is considered dose-dependent [57] and it is associated to an imbalance of cytoplasmic iron ions which may cause oxidative stress leading to cellular toxicity, impaired cell metabolism, and concomitant increment in apoptosis [58].

In such cases the level and nature of the coating material is considered a valid tool to minimize the toxic effects. In the present work, the selection of AA as coating offered several advantages such as its biodisponibility, low cost and biosafety. Besides, its effect as biocompatibility enhancer has been reported including *in vivo* assays by increasing cellular absorption of iron and decreasing their toxicity [59].

Moreover, as further qualitative evidence, the nanoparticles were visualized inside cells by bright field microscopy (see supplementary material, Figure S8). The image corresponds to the cells treated with the dose of 100 µg/ml, where the nanoparticles may be identified as light brown spots inside the cells. From the data on the **Figure 6a** and **S6**, it may infer that Mag-AA is not affecting the cell division or metabolic capacity of these cells even when the highest doses and incubation times are employed.

The toxicity of magnetic nanoparticles has been reported as dependent on size, surface charge and nature of coating. To assess the toxicity of nanoparticles not only in vitro but also in vivo studies should be performed. The former ones usually determine higher toxicity than the latest one. This is because during in vivo experiments possible toxic degradation products can be continuously eliminated from the body [60]. Future in vivo test are needed to determine the authentic potential toxicity of Mag-AA3, as well as their biodistribution. Those investigations will be matter of a next separate work.

3.2.2.   *Uptake of AA-Mag4 MNPs by HCT116 cells*

Prussian blue staining was employed to gain information on the MNPs uptake on HCT 116 cell. This staining method makes particles blue, and gives suitable contrast in the optical microscopes allowing a preliminary evaluation of the particles labeling efficacy. The results are depicted in **Figure 6b** indicating MNPs containing sites as light blue spots. MNPs internalized via formation of ferric ferrocyanide, by the reaction of Fe^{3+} with

$K_4Fe(CN)_6$ and the effect was determined as dose dependent. That means that the highest MNPs doses (100 µg Fe/ml Mag-AA3) leaded to a cell labeling efficiency of about 100%. Other authors have reported similar findings concerning the dose dependent up take level; and besides have shown the importance of the MNPs surface charge and coating in the up take efficiency [61]. Although it has been reported that positively charged nanoparticles are better internalized by cells, negatively charged ones, has been associated with lower toxicity[61].

In addition, iron determination inside the cell was achieved using atomic absorption spectroscopy as a complement of the qualitative determination by Prussian blue [62]. The Fe contents measured in cell pellets and cell supernatant are listed in **Table 2**.

Table 2. Iron content (Fe µg/ml) and the magnetite arising from it, from HCT116 cell cultures after incubation with different doses of Mag-AA. Percentage of cellular uptake is also shown.

The data on the table indicate that lower Mag-AA3 doses supply an undetectable amount of Fe on the cell structure, at least using atomic absorption spectroscopy. The highest doses ensured the presence of iron in almost all the isolated cell fractions. The results agree Prussian Blue observations, where more blue spots were detected with the dose of 100 µg/ml compared with the dose of 10 µg/ml.

The amount of Mag-AA3 found in cell supernatant could be considered as nanoparticles adsorbed on cellular surface. On the other hand, iron measured in cell pellets corresponds certainly to internalized nanoparticles [62]. Based on the data from atomic absorption spectroscopy, a quantitative measurement on the MNPs internalization may be achieved by using the highest dose. The sum of the cellular fractions (supernatant and pellets) revealed that a 17.75% of the total nanoparticles labelled the cells. From these nanoparticles, 36.6% were internalized while 63.4% remained adsorbed in cell surface.

As iron was not detected in all doses and fractions analyzed, it is not possible infer a trend regarding the dependency of nanoparticles dose. Even when the doses appears to be a key factor on the up take efficiency other factors such as hydrodynamic size, stability on the physiological media, cell type, number of treated cells and the duration of the experiment must also be considered to assess a rigorous analysis [63].

4. Concluding remarks

Water dispersible magnetic nanoparticles coated with organic acids were achieved by acutely adjusting the reaction conditions using co-precipitation method. The best formulation in terms of size and stability was the AA coated Mag, showing a stable hydrodynamic size during already three months. Mag-MA resulted in suitable properties concerning to size and surface charge but limited stability (already 12hs), being unsuitable for the desired applications.

Mag-AA formulations where explored in terms of the initial AA concentration, being MAG-AA3 the most suitable one. This formulation demonstrated to be efficient in generating the negative T_2 contrast as demonstrated the assays performed in the clinical RMI equipment.

In vitro assays on cancer colon rectal cell culture indicated that the cell viability was not affected even when incubating high concentrations of nanoparticles for 48 h. Besides, the Mag-AA3 uptake on HCT116 cells was demonstrated by two independent techniques, revealing the efficient MNPs internalization mainly at high-administrated doses.

The experiments carried out are the required preliminary stage in view of the future *in vivo* application in animal models to really validate the proposed magnetic formulation.

Acknowledgments

References

[1]   P.G. Camici, O.E. Rimoldi, O. Gaemperli, P. Libby, Non-invasive anatomic and functional imaging of vascular inflammation and unstable plaque, Eur. Heart J. 33 (2012) 1309–1317. doi:10.1093/eurheartj/ehs067.

[2]   J. Li, Nanotechnology-based platform for early diagnosis of cancer, Sci. Bull. 60 (2015) 488–490. doi:10.1007/s11434-014-0720-9.

[3]   H.S. Thomsen, Nephrogenic systemic fibrosis: a serious adverse reaction to gadolinium - 1997-2006-2016. Part 1, Acta Radiol. 57 (2016) 515–520. doi:10.1177/0284185115626480.

[4]   A.K. Abu-Alfa, Nephrogenic Systemic Fibrosis and Gadolinium-Based Contrast Agents, Adv. Chronic Kidney Dis. 18 (2011) 188–198. doi:10.1053/j.ackd.2011.03.001.

[5]   E.A. Neuwelt, B.E. Hamilton, C.G. Varallyay, W.R. Rooney, R.D. Edelman, P.M. Jacobs, S.G. Watnick, Ultrasmall superparamagnetic iron oxides (USPIOs): a future alternative magnetic resonance (MR) contrast agent for patients at risk for nephrogenic systemic fibrosis (NSF)?, Kidney Int. 75 (2009) 465–474. doi:10.1038/ki.2008.496.

[6]   J.P. Finn, K.L. Nguyen, P. Hu, Ferumoxytol vs. Gadolinium agents for contrast-enhanced MRI: Thoughts on evolving indications, risks, and benefits, J. Magn. Reson. Imaging. 46 (2017) 919–923. doi:10.1002/jmri.25580.

[7]   M.A. Busquets, J. Estelrich, M.J. Sánchez-Martín, Nanoparticles in magnetic resonance imaging: from simple to dual contrast agents, Int. J. Nanomedicine. 10 (2015) 1727. doi:10.2147/IJN.S76501.

[8]   Yi-Xiang J, Wang, Current status of superparamagnetic iron oxide contrast agents for liver magnetic resonance imaging, World J. Gastroenterol. 21 (2015) 13400–13402. doi:10.3748/wjg.v21.i47.13400.

[9]   Lima-Tenório, M. K., G. Pineda, E. A., N.M. Ahmad, H. Fessi, A. Elaissari, Magnetic nanoparticles: In vivo cancer diagnosis and therapy, Int. J. Pharm. 493 (2015) 313–327. doi:10.1016/j.ijpharm.2015.07.059.

[10]   K. El-Boubbou, D.C. Zhu, C. Vasileiou, B. Borhan, D. Prosperi, W. Li, X. Huang, Magnetic Glyco-Nanoparticles: A Tool To Detect, Differentiate,\rand Unlock the Glyco-Codes of Cancer via Magnetic\rResonance Imaging, J. Am. Chem. Soc. 132 (2010) 4490–4499. doi:10.1021/ja100455c.

[11]   J. Li, Y. He, W. Sun, Y. Luo, H. Cai, Y. Pan, M. Shen, J. Xia, X. Shi, Hyaluronic

acid-modified hydrothermally synthesized iron oxide nanoparticles for targeted tumor MR imaging, Biomaterials. 35 (2014) 3666–3677. doi:10.1016/j.biomaterials.2014.01.011.

[12] R.G. Thomas, M.J. Moon, H. Lee, A.R.K. Sasikala, C.S. Kim, I.K. Park, Y.Y. Jeong, Hyaluronic acid conjugated superparamagnetic iron oxide nanoparticle for cancer diagnosis and hyperthermia therapy, Carbohydr. Polym. 131 (2015) 439–446. doi:10.1016/j.carbpol.2015.06.010.

[13] M.H. El-Dakdouki, K. El-Boubbou, M. Kamat, R. Huang, G.S. Abela, M. Kiupel, D.C. Zhu, X. Huang, CD44 targeting magnetic glyconanoparticles for atherosclerotic plaque imaging, Pharm. Res. 31 (2014) 1426–1437. doi:10.1007/s11095-013-1021-8.

[14] W. Liu, L. Nie, F. Li, Z.P. Aguilar, H. Xu, Y. Xiong, F. Fu, H. Xu, Folic acid conjugated magnetic iron oxide nanoparticles for nondestructive separation and detection of ovarian cancer cells from whole blood, Biomater. Sci. 4 (2016) 159–166. doi:10.1039/C5BM00207A.

[15] M. Suzuki, L. Bachelet-Violette, F. Rouzet, A. Beilvert, G. Autret, M. Maire, C. Menager, L. Louedec, C. Choqueux, P. Saboural, O. Haddad, C. Chauvierre, F. Chaubet, J.-B. Michel, J.-M. Serfaty, D. Letourneur, Ultrasmall superparamagnetic iron oxide nanoparticles coated with fucoidan for molecular MRI of intraluminal thrombus, Nanomedicine. 10 (2015) 73–87. doi:10.2217/nnm.14.51.

[16] C. Scharlach, H. Kratz, F. Wiekhorst, C. Warmuth, J. Schnorr, G. Genter, M. Ebert, S. Mueller, E. Schellenberger, Synthesis of acid-stabilized iron oxide nanoparticles and comparison for targeting atherosclerotic plaques: Evaluation by MRI, quantitative MPS, and TEM alternative to ambiguous Prussian blue iron staining, Nanomedicine Nanotechnology, Biol. Med. 11 (2015) 1–11. doi:10.1016/j.nano.2015.01.002.

[17] R. Hachani, M. Lowdell, M. Birchall, A. Hervault, D. Mertz, S. Begin-Colin, N.T.K. Thanh, Polyol synthesis, functionalisation, and biocompatibility studies of superparamagnetic iron oxide nanoparticles as potential MRI contrast agents, Nanoscale. 8 (2016) 3278–3287. doi:10.1039/C5NR03867G.

[18] S. Cammas-Marion, M.M. Bear, A. Harada, P. Guerin, K. Kataoka, New macromolecular micelles based on degradable amphiphilic block copolymers of malic acid and malic acid ester, Macromol. Chem. Phys. 201 (2000) 355–364.

doi:10.1002/(sici)1521-3935(20000201)201:3<355::aid-macp355>3.0.co;2-9.

[19] S. Chambial, S. Dwivedi, K.K. Shukla, P.J. John, P. Sharma, Vitamin C in disease prevention and cure: An overview, Indian J. Clin. Biochem. 28 (2013) 314–328. doi:10.1007/s12291-013-0375-3.

[20] D.B. Agus, J.C. Vera, D.W. Golde, Stromal Cell Oxidation : A Mechanism by Which Tumors Obtain Vitamin C Advances in Brief Stromal Cell Oxidation : A Mechanism by Which Tumors Obtain Vitamin C 1, Cancer Res. 10021 (1999) 4555–4558.

[21] S.C. Rumsey, O. Kwon, G.W. Xu, C.F. Burant, I. Simpson, M. Levine, Glucose transporter isoforms GLUT1 and GLUT3 transport dehydroascorbic acid, J. Biol. Chem. 272 (1997) 18982–18989. doi:10.1074/jbc.272.30.18982.

[22] V.L. Lassalle, R.D. Zysler, M.L. Ferreira, Novel and facile synthesis of magnetic composites by a modified co-precipitation method, Mater. Chem. Phys. 130 (2011) 624–634. doi:10.1016/j.matchemphys.2011.07.035.

[23] P. Azcona, R. Zysler, V. Lassalle, Simple and novel strategies to achieve shape and size control of magnetite nanoparticles intended for biomedical applications, Colloids Surfaces A Physicochem. Eng. Asp. 504 (2016) 320–330. doi:10.1016/j.colsurfa.2016.05.064.

[24] J. Yan, S. Mo, J. Nie, W. Chen, X. Shen, J. Hu, G. Hao, H. Tong, Hydrothermal synthesis of monodisperse Fe3O4 nanoparticles based on modulation of tartaric acid, Colloids Surfaces A Physicochem. Eng. Asp. 340 (2009) 109–114. doi:10.1016/j.colsurfa.2009.03.016.

[25] H. Gupta, P. Paul, N. Kumar, S. Baxi, D.P. Das, One pot synthesis of water-dispersible dehydroascorbic acid coated Fe3O4 nanoparticles under atmospheric air: Blood cell compatibility and enhanced magnetic resonance imaging, J. Colloid Interface Sci. 430 (2014) 221–228. doi:10.1016/j.jcis.2014.05.043.

[26] G. Garrido, C. Ràfols, E. Bosch, Acidity constants in methanol/water mixtures of polycarboxylic acids used in drug salt preparations: Potentiometric determination of aqueous pK a values of quetiapine formulated as hemifumarate, Eur. J. Pharm. Sci. 28 (2006) 118–127. doi:10.1016/j.ejps.2006.01.005.

[27] J J Max, C. Chapados, Infrared spectroscopy of carboxilic acids: Malic acid, J. Phys. Chem. A. 106 (2002) 6452.

[28] V. Sreeja, K.N. Jayaprabha, P.A. Joy, Water-dispersible ascorbic-acid-coated magnetite nanoparticles for contrast enhancement in MRI, Appl. Nanosci. 5

(2015) 435–441. doi:10.1007/s13204-014-0335-0.

[29]   V. Salvadó, X. Ribas, M. Blanco, M. Valiente, On the chemistry of iron in biosystems. I. Complex formation between Fe(III) and tartaric acid: a "core + link" mechanism, Inorganica Chim. Acta. 137 (1987) 155–159. doi:10.1016/S0020-1693(00)81159-7.

[30]   A. De Luca, R.F. Dantas, S. Esplugas, Assessment of iron chelates efficiency for photo-Fenton at neutral pH, Water Res. 61 (2014) 232–242. doi:10.1016/j.watres.2014.05.033.

[31]   Y. Kuwahara, T. Miyazaki, Y. Shirosaki, G. Liu, M. Kawashita, Structures of organic additives modified magnetite nanoparticles, Ceram. Int. 42 (2016) 6000–6004. doi:10.1016/j.ceramint.2015.12.152.

[32]   S.D. Bohnenstiehl, M.A. Susner, Y. Yang, E.W. Collings, M.D. Sumption, M.A. Rindfleisch, R. Boone, Carbon doping of MgB2 by toluene and malic-acid-in-toluene, Phys. C. 471 (2011) 108–111. doi:10.1016/j.physc.2010.12.005.

[33]   S. Prakash Parthiban, K. Elayaraja, E.K. Girija, Y. Yokogawa, R. Kesavamoorthy, M. Palanichamy, K. Asokan, S. Narayana Kalkura, Preparation of thermally stable nanocrystalline hydroxyapatite by hydrothermal method, J. Mater. Sci. Mater. Med. 20 (2009) S77–S83. doi:10.1007/s10856-008-3484-4.

[34]   M. Juhász, Y. Kitahara, S. Takahashi, T. Fujii, Thermal stability of vitamin C: Thermogravimetric analysis and use of total ion monitoring chromatograms, J. Pharm. Biomed. Anal. 59 (2012) 190–193. doi:10.1016/j.jpba.2011.10.011.

[35]   L. Xiao, J. Li, D.F. Brougham, E.K. Fox, N. Feliu, A. Bushmelev, N. Mertens, F. Kiessling, M. Valldor, B. Fadeel, S. Mathur, Water-Soluble Superparamagnetic Magnetite Nanoparticles with Biocompatible Coating for Enhanced Magnetic Resonance Imaging (MRI) Water-Soluble Superparamagnetic Magnetite Nanoparticles with Biocompatible Coating for Enhanced Magnetic Resonance Imaging (, ACS Nano. 5 (2011) 6315–6324. doi:10.1021/nn201348s.

[36]   M. Agotegaray, A. Campelo, R. Zysler, F. Gumilar, C. Bras, A. Minetti, V. Massheimer, V. Lassalle, Influence of chitosan coating on magnetic nanoparticles in endothelial cells and acute tissue biodistribution, J. Biomater. Sci. Polym. Ed. 27 (2016) 1069–1085. doi:10.1080/09205063.2016.1170417.

[37]   M.F. Horst, D.F. Coral, M.B. Fernández van Raap, M. Alvarez, V. Lassalle, Hybrid nanomaterials based on gum Arabic and magnetite for hyperthermia treatments, Mater. Sci. Eng. C. 74 (2017) 443–450. doi:10.1016/j.msec.2016.12.035.

[38] I. Karimzadeh, H. Dizaji Rezagholipour, M. Aghazadeh, Development of a facile and effective electrochemical strategy for preparation of iron oxides (Fe 3 O 4 and γ -Fe 2 O 3) nanoparticles from aqueous and ethanol mediums and in situ PVC coating of Fe 3 O 4 superparamagnetic nanoparticles for biomedical ap, J. Magn. Magn. Mater. 416 (2016) 81–88. doi:10.1016/j.jmmm.2016.05.015.

[39] W. Wu, Z. Wu, T. Yu, C. Jiang, W.-S. Kim, Recent progress on magnetic iron oxide nanoparticles: synthesis, surface functional strategies and biomedical applications, Sci. Technol. Adv. Mater. 16 (2015) 023501. doi:10.1088/1468-6996/16/2/023501.

[40] M. Mahdavi, M. Bin Ahmad, M.J. Haron, F. Namvar, B. Nadi, M.Z. Ab Rahman, J. Amin, Synthesis, surface modification and characterisation of biocompatible magnetic iron oxide nanoparticles for biomedical applications, Molecules. 18 (2013) 7533–7548. doi:10.3390/molecules18077533.

[41] J. Qu, G. Liu, Y. Wang, R. Hong, Preparation of Fe3O4-chitosan nanoparticles used for hyperthermia, Adv. Powder Technol. 21 (2010) 461–467. doi:10.1016/j.apt.2010.01.008.

[42] M.E. de Sousa, M.B. Fernández van Raap, P.C. Rivas, P. Mendoza Zélis, P. Girardin, G.A. Pasquevich, J.L. Alessandrini, D. Muraca, F.H. Sánchez, Stability and Relaxation Mechanisms of Citric Acid Coated Magnetite Nanoparticles for Magnetic Hyperthermia, J. Phys. Chem. C. 117 (2013) 5436–5445. doi:10.1021/jp311556b.

[43] P. Nicolás, M. Saleta, H. Troiani, R. Zysler, V. Lassalle, M.L. Ferreira, Preparation of iron oxide nanoparticles stabilized with biomolecules: Experimental and mechanistic issues, Acta Biomater. 9 (2013) 4754–4762. doi:10.1016/j.actbio.2012.09.040.

[44] D. Ramimoghadam, S. Bagheri, S. Hamid Abd, Bee, Journal of Magnetism and Magnetic Materials, J. Magn. Magn. Mater. 379 (2015) 74–79. doi:10.1016/j.jmmm.2014.12.005 0304-8853/&.

[45] Y.P. Hsieh, Y.P. Hsieh, Kinetics of Fe (III) Reduction by Ascorbic Acid in Aqueous Solutions, J. Agric. Food Chem. 48 (2000) 1569–1573. doi:10.1021/jf9904362.

[46] H.-C. Roth, S.P. Schwaminger, M. Schindler, F.E. Wagner, S. Berensmeier, Influencing factors in the CO-precipitation process of superparamagnetic iron oxide nano particles: A model based study, J. Magn. Magn. Mater. 377 (2015)

81–89. doi:10.1016/j.jmmm.2014.10.074.

[47] E. Illés, M. Szekeres, E. Kupcsik, I.Y. Tóth, K. Farkas, A. Jedlovszky-hajdú, E. Tombácz, PEGylation of surfacted magnetite core – shell nanoparticles for biomedical application, Colloids Surfaces A Physicochem. Eng. Asp. 460 (2014) 429–440. doi:10.1016/j.colsurfa.2014.01.043.

[48] T.K. Jain, J. Richey, M. Strand, D.L. Leslie-Pelecky, C.A. Flask, V. Labhasetwar, Magnetic nanoparticles with dual functional properties: Drug delivery and magnetic resonance imaging, Biomaterials. 29 (2008) 4012–4021. doi:10.1016/j.biomaterials.2008.07.004.

[49] Y.-X.J. Wang, Superparamagnetic iron oxide based MRI contrast agents: Current status of clinical application, Quant Imaging Med Surg. 1 (2011) 35–44. doi:10.3978/j.issn.2223-4292.2011.08.03.

[50] N. Lee, T. Hyeon, Designed synthesis of uniformly sized iron oxide nanoparticles for efficient magnetic resonance imaging contrast agents, Chem. Soc. Rev. 41 (2012) 2575–2589. doi:10.1039/C1CS15248C.

[51] C. Kaittanis, S. Santra, O.J. Santiesteban, T.J. Henderson, J.M. Perez, The assembly state between magnetic nanosensors and their targets orchestrates their magnetic relaxation response, J. Am. Chem. Soc. 133 (2011) 3668–3676. doi:10.1021/ja1109584.

[52] E. Taboada, R. Solanas, E. Rodríguez, R. Weissleder, A. Roig, Supercritical-fluid-assisted one-pot synthesis of biocompatible core(γ-Fe2O3)/shell(SiO2) nanoparticles as high relaxivity T2-contrast agents for magnetic resonance imaging, Adv. Funct. Mater. 19 (2009) 2319–2324. doi:10.1002/adfm.200801681.

[53] Mosmann T., Rapid colorimetric assay for cellular growth and survival: Application to proliferation and cytotoxicity assays, J. Immunol. Meth. 65 (1983) 55–63.

[54] E. Aşık, Y. Akpınar, N.T. Güray, M. İşcan, G.Ç. Demircigil, M. Volkan, Cellular uptake, genotoxicity and cytotoxicity of cobalt ferrite magnetic nanoparticles in human breast cells, Toxicol. Res. (Camb). 5 (2016) 1649–1662. doi:10.1039/C6TX00211K.

[55] M. Mahmoudi, A. Simchi, A.S. Milani, P. Stroeve, Cell toxicity of superparamagnetic iron oxide nanoparticles, J. Colloid Interface Sci. 336 (2009) 510–518. doi:10.1016/j.jcis.2009.04.046.

[56] M. Marcus, M. Karni, K. Baranes, I. Levy, N. Alon, S. Margel, O. Shefi, Iron oxide nanoparticles for neuronal cell applications: uptake study and magnetic

manipulations., J. Nanobiotechnology. 14 (2016) 37. doi:10.1186/s12951-016-0190-0.

[57] C. Boyer, M.R. Whittaker, V. Bulmus, J. Liu, T.P. Davis, The design and utility of polymer-stabilized iron-oxide nanoparticles for nanomedicine applications, NPG Asia Mater. 2 (2010) 23–30. doi:10.1038/asiamat.2010.6.

[58] J. Hall, Guyton and Hall Textbook of Medical Physiology, 13th ed., Elsevier Inc., Philadelphia, 2015.

[59] H. Bassiony, S. Sabet, T.A.S. El-Din, M.M. Mohamed, A.A. El-Ghor, Magnetite nanoparticles inhibit tumor growth and upregulate the expression of P53/P16 in Ehrlich solid carcinoma bearing mice, PLoS One. 9 (2014) 1–9. doi:10.1371/journal.pone.0111960.

[60] G. Kania, M. Sternak, A. Jasztal, S. Chlopicki, A. Błażejczyk, A. Nasulewicz-Goldeman, J. Wietrzyk, K. Jasiński, T. Skórka, S. Zapotoczny, M. Nowakowska, Uptake and bioreactivity of charged chitosan-coated superparamagnetic nanoparticles as promising contrast agents for magnetic resonance imaging, Nanomedicine Nanotechnology, Biol. Med. 14 (2018) 131–140. doi:10.1016/j.nano.2017.09.004.

[61] M. Calero, L. Gutiérrez, G. Salas, Y. Luengo, A. Lázaro, P. Acedo, M.P. Morales, R. Miranda, A. Villanueva, Efficient and safe internalization of magnetic iron oxide nanoparticles: Two fundamental requirements for biomedical applications, Nanomedicine Nanotechnology, Biol. Med. 10 (2014) 733–743. doi:10.1016/j.nano.2013.11.010.

[62] S.I.C.J. Palma, C.A. V. Rodrigues, A. Carvalho, M. del P. Morales, F. Freitas, A.R. Fernandes, J.M.S. Cabral, A.C.A. Roque, A value-added exopolysaccharide as a coating agent for MRI nanoprobes, Nanoscale. 7 (2015) 14272–14283. doi:10.1039/C5NR01979F.

[63] V. Némethová, B. Buliaková, P. Mazancová, A. Bábelová, M. Šelc, D. Moravčíková, L. Kleščíková, M. Ursínyová, A. Gábelová, F. Rázga, Intracellular uptake of magnetite nanoparticles: A focus on physico-chemical characterization and interpretation of in vitro data, Mater. Sci. Eng. C. 70 (2017) 161–168. doi:10.1016/j.msec.2016.08.064.

Figure 1. a) IR spectra of raw acids. b) IR spectra of the stabilized MNPs with AA, MA and TA.
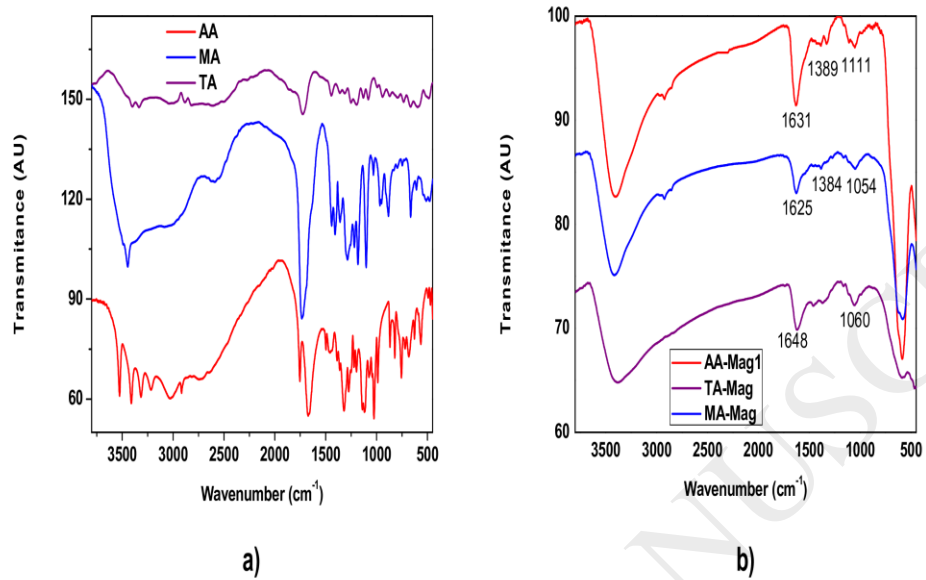
Figure 1

Figure 2. TEM micrographies of Mag-TA, Mag-MA and Mag-AA nanoparticles.
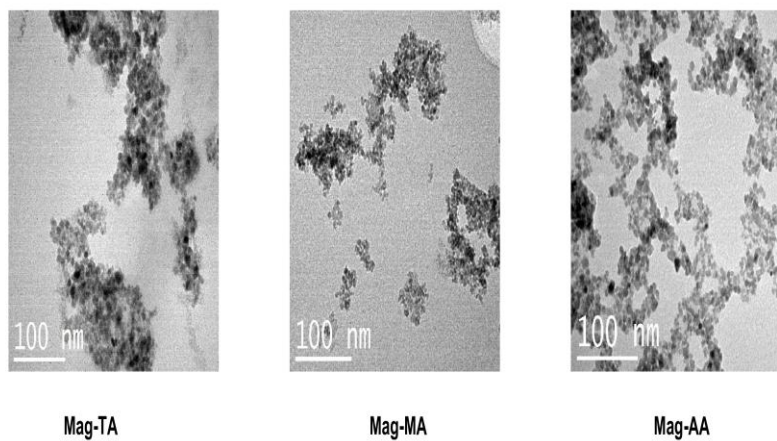
Mag-TA   Mag-MA   Mag-AA

Figure 2

Figure 3. a) XRD difractograms of Mag-TA, Mag-MA and Mag-AA1. b) Magnetic measurements by VSM of Mag-TA-Mag-MA and Mag-AA1.

a)

b)

Figure 3
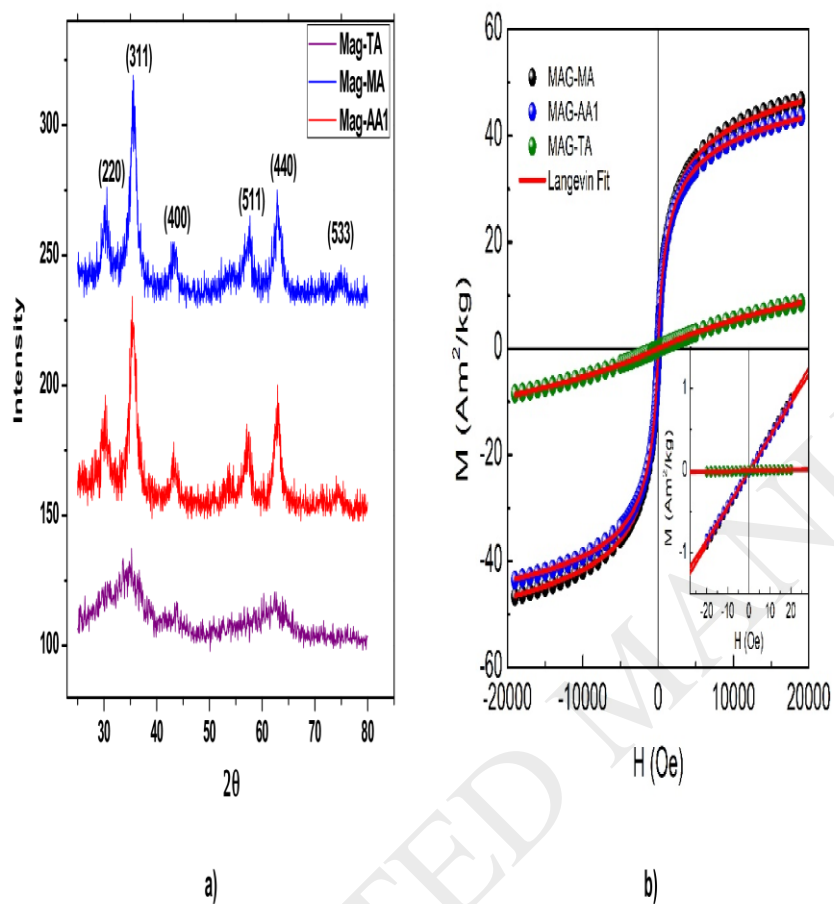
Figure 4. a) Hydrodynamic diameter (PDI: 0.218; 0.137; and 0.185 using 300, 600 and 900 mg of ascorbic acid respectively) and Z potential as a function of the nominal AA concentration. b) HR TEM of Mag-AA.
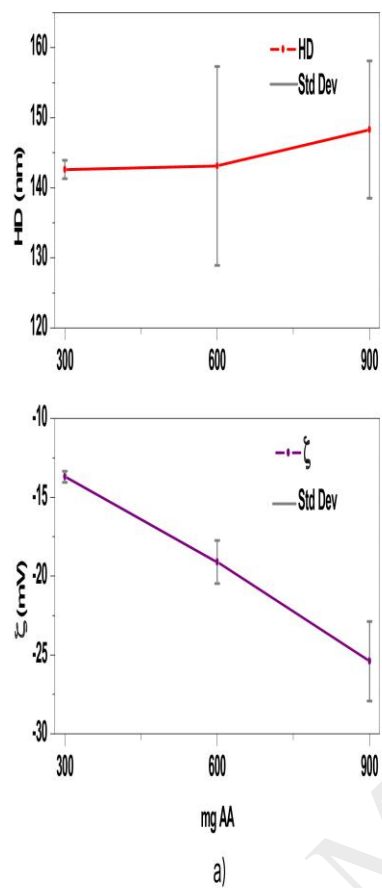

a)

b)
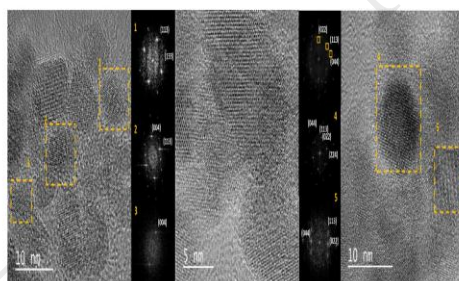
Figure 4

Figure 5. a) T_2-weighted images of Mag-AA3 with a TE= 250ms and TR= 2000ms. b) Transverse relaxation rate vs iron concentration, the slope represents r2.
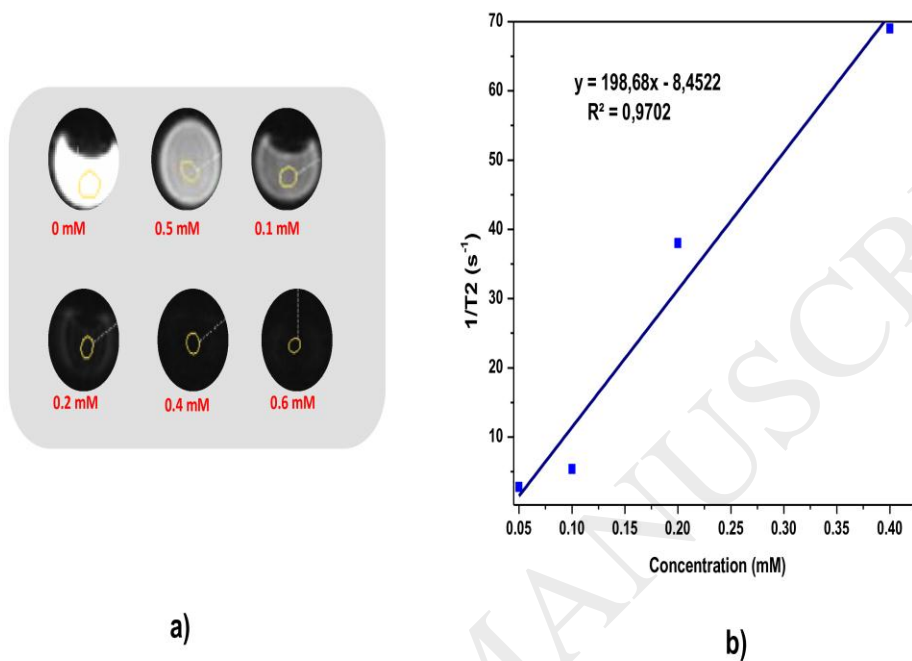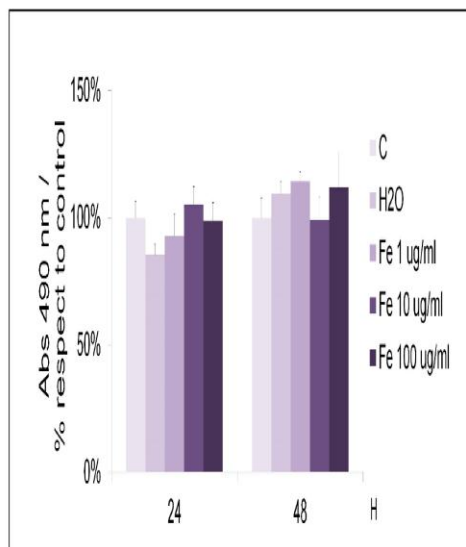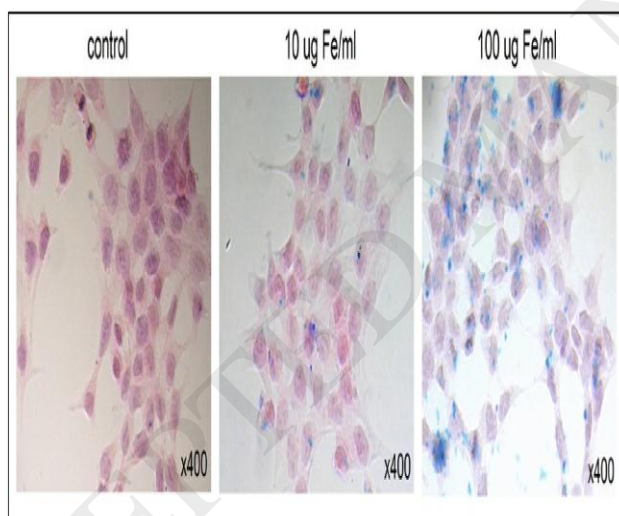

a)

$y = 198,68x - 8,4522$
$R^2 = 0,9702$

b)

Figure 5

Figure 6. a) Cell viability assay results for HCT116 cell line after 24h Mag-AA3 nanoparticles. Data is expressed as mean ± standard deviation of two independent experiments. b) Prussian Blue staining in HCT116 cells treated with different concentrations of Mag-AA3 nanoparticles. Magnification 400x.

a)

b)

Figure 6

Table 1. Data on hydrodynamic diameter by DLS with the corresponding PDI and TEM estimated magnetic core size as a function of the coating.

Formulation	TEM estimated diameter (nm)	Hydrodynamic diameter (nm)	PDI	ζ (mv)
Naked Magnetite *	n.d	417	0.252	-8.48
Mag-TA	7.5 ± 0.05	148.1± 3.94	0.228	-28 ± 0.15
Mag-MA	8.5 ± 1.55	94.8 ± 3.74	0.141	-17,1± 2.40
Mag-AA1	8.5 ± 1.86	143.1± 14.2	0.137	-18.6 ± 1.36

*Ref: [43]

n.d: Not determined due to the presence of large aggregates

Table 2. Iron content (Fe µg/ml) and the MNPs arising from it, from HCT116 cell cultures after incubation with different doses of Mag-AA. Percentage of cellular uptake is also shown.

Sample	Fe (µg/ml)	µg of MNPs*	% MNPs cell uptake
Cell supernatant control	No detected	-----	----
Cell supernatant 1 µg/ml	No detected	-----	----
Cell supernatant 10 µg/ml	0.07	1,1	5.5%
Cell supernatant 100 µg/ml	1.63	24.7	12.35%
Cells pellts control	No detected	-----	----
Cells pellets 1 µg/ml	No detected	-----	----
Cells pellets 10 µg/ml	No detected	-----	----
Cells pellets 100 µg/ml	1	15	7.5%

*In 10mL that represents the total volume of each sample